Phase Segregation of Untethered Zwitterionic Model Lipid Bilayers Observed on Mercaptoundecanoic-Acid-Modified Gold by AFM Imaging

ARTICLE *in* LANGMUIR · APRIL 2010

Impact Factor: 4.46 · DOI: 10.1021/la100605t · Source: PubMed

3 AUTHORS, INCLUDING:

James K Li
University of Toronto
18 PUBLICATIONS **194** CITATIONS
SEE PROFILE

Gilbert C. Walker
University of Toronto
172 PUBLICATIONS **5,007** CITATIONS
SEE PROFILE

Langmuir
Article
pubs.acs.org/Langmuir

Phase Segregation of Untethered Zwitterionic Model Lipid Bilayers Observed on Mercaptoundecanoic-Acid-Modified Gold by AFM Imaging and Force Mapping

Shell Ip, James K. Li, and Gilbert C. Walker*

Department of Chemistry, University of Toronto, Ontario, Canada

Received February 9, 2010. Revised Manuscript Received March 25, 2010

Planar supported lipid bilayers (SLBs) are often studied as model cell membranes because they are accessible to a variety of surface-analytic techniques. Specifically, recent studies of lipid phase coexistence in model systems suggest that membrane lateral organization is important to a range of cellular functions and diseases. We report the formation of phase-segregated dioleoylphosphatidylcholine (DOPC)/sphingomyelin/cholesterol bilayers on mercaptoundecanoic-acid-modified (111) gold by spontaneous fusion of unilamellar vesicles, without the use of charged or chemically modified headgroups. The liquid-ordered (l_o) and liquid-disordered (l_d) domains are observed by atomic force microscopy (AFM) height and phase imaging. Furthermore, the mechanical properties of the bilayer were characterized by force−indentation maps. Fits of force indentation to Sneddon mechanics yields average apparent Young's moduli of the l_o and l_d phases of 100 ± 2 and 59.8 ± 0.9 MPa, respectively. The results were compared to the same lipid membrane system formed on mica with good agreement, though modulus values on mica appeared higher. Semiquantitative comparisons suggest that the mechanical properties of the l_o phase are dominated by intermolecular van der Waals forces, while those of the fluid l_d phase, with relatively weak van der Waals forces, are influenced appreciably by differences in surface charge density between the two substrates, which manifests as a difference in apparent Poisson ratios.

Introduction

Planar supported lipid bilayers (SLBs) are often studied as model cell membranes because they are accessible to a variety of surface-analytic techniques, such as scanned-probe microscopy,[1−6] fluorescence microscopy,[7−9] electrical impedance analysis,[10,11] time-of-flight secondary ion mass spectrometry,[12] and neutron scattering,[13] that allow detailed characterization of membrane morphology. Such characterization has been widely employed to study model lipid systems that phase segregate into coexisting liquid-ordered and liquid-disordered phases. The coexistence of different lipid phases is of fundamental importance to the raft hypothesis for cellular membranes, which over the last 15 years has evolved as a model for the lateral organization and heterogeneity of cell membranes, which has been found to play a role in processes such as cell signaling[14−18] and also in mechanisms of diseases such as Alzheimer's[19,20] and HIV/AIDS.[21,22]

Furthermore, studies on model systems show that inhomogeneous receptor distribution on surfaces at length scales comparable to rafts profoundly affects the morphology of cells bound to these surfaces.[23−26] Thus, the role of phase segregation and more specifically its effect on receptor distribution and membrane interactions with cells, drugs, and viruses may be better understood by further characterization using diverse methods.

Specifically, surface plasmon resonance (SPR) and related plasmonic techniques are suitable for studying the kinetics of interactions between soluble ligands and membrane-bound proteins or the membrane itself.[27−30] Additionally, lipid bilayers have been identified as a possible platform for surface functionalization

*To whom correspondence should be addressed. E-mail: gilbert.walker@utoronto.ca.

(1) Johnston, L. J. *Langmuir* **2007**, *23*, 5886–5895.
(2) Connell, S. D.; Smith, D. A. *Mol. Membr. Biol.* **2006**, *23*, 17–28.
(3) Dufrêne, Y. F.; Lee, G. U. *Biochim. Biophys. Acta, Biomembr.* **2000**, *1509*, 14–41.
(4) Kruger, S.; Kruger, D.; Janshoff, A. *ChemPhysChem* **2004**, *5*, 989–997.
(5) Slade, A.; Luh, J.; Ho, S.; Yip, C. M. *J. Struct. Biol.* **2002**, *137*, 283–291.
(6) Hollars, C. W.; Dunn, R. C. *Biophys. J.* **1998**, *75*, 342–353.
(7) Korlach, J.; Schwille, P.; Webb, W.; Feigenson, G. *Proc. Natl. Acad. Sci. U.S.A.* **1999**, *96*, 8461–8466.
(8) Mattjus, P.; Slotte, J. P. *Chem. Phys. Lipids* **1996**, *81*, 69–80.
(9) Chiantia, S.; Ries, J.; Schwille, P. *Biochim. Biophys. Acta, Biomembr.* **2009**, *1788*, 225–233.
(10) Steinem, C.; Janshoff, A.; Galla, H.; Sieber, M. *Bioelectrochem. Bioenerg.* **1997**, *42*, 213–220.
(11) Steinem, C.; Janshoff, A.; Ulrich, W. P.; Sieber, M.; Galla, H. J. *Biochim. Biophys. Acta, Biomembr.* **1996**, *1279*, 169–180.
(12) Kraft, M. L.; Weber, P. K.; Longo, M. L.; Hutcheon, I. D.; Boxer, S. G. *Science* **2006**, *313*, 1948–1951.
(13) Johnson, S.; Bayerl, T.; McDermott, D.; Adam, G.; Rennie, A.; Thomas, R.; Sackmann, E. *Biophys. J.* **1991**, *59*, 289–294.
(14) London, E.; Brown, D. *Biochim. Biophys. Acta, Biomembr.* **2000**, *1508*, 182–195.
(15) Brown, D.; London, E. *J. Membr. Biol.* **1998**, *164*, 103–114.
(16) Brown, D. A.; London, E. *Annu. Rev. Cell. Dev. Biol.* **1998**, *14*, 111–136.
(17) Simons, K.; Vaz, W. L. *Annu. Rev. Biophys. Biomol. Struct.* **2004**, *33*, 269–295.
(18) Stillwell, W.; Shaikh, S. R.; Zerouga, M.; Siddiqui, R.; Wassall, S. R. *Reprod., Nutr., Dev.* **2005**, *45*, 21.
(19) Wong, P.; Schauerte, J.; Wisser, K.; Ding, H.; Lee, E.; Steel, D.; Gafni, A. *J. Mol. Biol.* **2009**, *386*, 81–96.
(20) D'Errico, G.; Vitiello, G.; Ortona, O.; Tedeschi, A.; Ramunno, A.; D'Ursi, A. *Reprod. Nutr. Dev.* **2008**, *1778*, 2710–2716.
(21) Liao, Z.; Graham, D. R.; Hildreth, J. E. K. *AIDS Res. Hum. Retroviruses* **2003**, *19*, 675–687.
(22) Campbell, S. M.; Crowe, S. M.; Mak, J. *J. Clin. Virol.* **2001**, *22*, 217–227.
(23) Werbin, J. L.; Heinz, W. F.; Romer, L. H.; Hoh, J. H. *Langmuir* **2007**, *23*, 10883–10886.
(24) Santore, M. M.; Kozlova, N. *Langmuir* **2007**, *23*, 4782–4791.
(25) Mossman, K. D.; Campi, G.; Groves, J. T.; Dustin, M. L. *Science* **2005**, *310*, 1191–1193.
(26) Yu, J.; Nolting, B.; Tan, Y.; L, X.; Grvay-Hague, J.; Liu, G. *NanoBiotechnology* **2005**, *1*, 201–210.
(27) Plant, A. L.; Brighamburke, M.; Petrella, E. C.; Oshannessy, D. J. *Anal. Biochem.* **1995**, *226*, 342–348.
(28) Tawa, K.; Morigaki, K. *Biophys. J.* **2005**, *89*, 2750–2758.
(29) Jonsson, M. P.; Jonsson, P.; Dahlin, A. B.; Hook, F. *Nano Lett.* **2007**, *7*, 3462–3468.
(30) Salamon, Z.; Macleod, H. A.; Tollin, G. *Biochim. Biophys. Acta, Rev. Biomembr.* **1997**, *1331*, 131–152.

in biosensor applications.[29,31−33] The use and relevance of SPR and related biosensing platforms to this problem would be improved by the ability to spontaneously form bilayers of model, raft-forming lipid mixtures capable of inhomogeneous receptor display, such as those containing dioleoylphosphatidyl choline (DOPC), sphingomyelin, and cholesterol, on noble-metal surfaces required for SPR. Instead, most studies utilize lipid membrane systems with charged or chemically modified headgroups, unlike most found in nature, due to limitations in producing lipid bilayers on metal surfaces.[11] Furthermore, phase segregation and lateral heterogeneity, to our knowledge, have not been adequately demonstrated on metals. Phase segregated lipids on metals may also be relevant to other characterizations methods that require conductive surfaces, such as scanning tunneling microscopy, which has already been employed to study lipids.[34−36]

On glass or mica surfaces, preparation of raft-forming model membranes is routine and widely reported.[1,2,37−41] The vesicle fusion method, for example, is straightforward: SLBs are self-assembled when unilamellar vesicles adsorb to a hydrophilic surface and spontaneously rupture, fusing together to form a laterally mobile bilayer.[42−46,41] On metallic surfaces suitable for SPR or similar analytic techniques, bilayer formation (by vesicle fusion or otherwise) often requires a specific headgroup charge or chemical modification[11] to promote a favorable interaction with the metal surface. Methods of spontaneous SLB formation on metals are diverse: (1) Lipid monolayers can be deposited on top of a hydrophobic alkanethiol monolayer preformed on the metal surface to produce a hybrid bilayer.[27,47] This precludes the incorporation of transmembrane proteins into the layer that require hydration of both intracellular and extracellular domains. (2) The inner leaflet of the bilayer is anchored to the gold surface through proteins.[48] The anchoring at high concentrations reduces the lateral mobility of the SLB.[49] (3) SLBs containing lipids with cationic or anionic headgroups are formed spontaneously on gold surfaces with anionic or cationic surface modifications, respectively.[10,50] Strong electrostatic interactions, for example, between cationic lipids and negatively charged mica, have been shown to greatly reduce lateral mobility and result in abnormal phase boundaries.[51] (4) Vesicles can spontaneously fuse on the end of a gold wire freshly cut in a suspension of vesicles.[52] This system, however, is not suitable for SPR sensing. (5) Long chemisorbed tether molecules have been employed to produce bilayers with a larger aqueous compartment between the inner leaflet and the substrate. In principle, this method is suitable for the incorporation of transmembrane proteins with considerable cytosolic or extracellular domains,[53,54] but to our knowledge phase segregation has not been demonstrated on such a system. However, phase segregation has been demonstrated on similar systems using glass and quartz substrates,[55,56] and considering the degree to which the lipids are decoupled from the substrate, such a strategy could potentially produce phase-segregated bilayers on gold as well. In the present study, we demonstrate the phase segregation of untethered ternary lipid bilayers on gold, which are more directly analogous to the widely studied ternary lipid bilayers on mica.

Specifically, we report the formation of biologically relevant ternary lipid bilayers on mercaptoundecanoic-acid-modified (111) gold by spontaneous fusion of unilamellar vesicles, without the use of lipids bearing charged or chemically modified headgroups. Furthermore, we observe the phase segregation of the lipid into sphingomyelin-enriched liquid-ordered domains (l_o) and DOPC-enriched liquid-disordered domains (l_d) by atomic force microscopy. We also characterize the bilayer by force−indentation maps and compare the data to the identical lipid membrane system formed on mica, and we found good agreement in terms of the magnitudes of the apparent Young's moduli of the two phases. While there have been other studies that have demonstrated the deposition of neutral phospholipid bilayers on Au(111) surfaces[57,58] and phospholipid/cholesterol mixtures,[58,59] the lipid systems employed, as in many cases, are not known to phase segregate and are not, a priori, suitable for studying the functional consequences of lipid domain formation. Furthermore, the imaging and mechanical characterization of lipid phases on gold supports has not, to our knowledge, been examined. To achieve this, two limitations were overcome: (1) Bare-gold surfaces are prone to contamination, which quickly reduces the hydrophilicity beyond a range where vesicle fusion can occur, and (2) direct observation of lipid phase segregation by scanned-probe microscopy is difficult on thermally deposited gold because the roughness is on the length scale of the lipid bilayer thickness. To address the first, we modify the gold with mercaptoundecanoic acid (MUDA), which makes the surface negatively charged much like freshly cleaved mica, and the surface remains hydrophilic much longer than bare gold. To address the second, we flame-anneal the gold prior to MUDA deposition to produce large (several square micrometers) single-crystal faces with RMS roughnesses that are an order of magnitude lower than that of as-deposited gold. These methods can be extended to prepare bilayers on generic gold surfaces.

(31) Watts, T. H.; Gaub, H. E.; McConnell, H. M. *Nature* **1986**, *320*, 179–181.
(32) Castellana, E. T.; Cremer, P. S. *Surf. Sci. Rep.* **2006**, *61*, 429–444.
(33) Avery, C. W.; Som, A.; Xu, Y.; Tew, G. N.; Chen, Z. *Anal. Chem.* **2009**, *81*, 8365–8372.
(34) Sek, S.; Laredo, T.; Dutcher, J. R.; Lipkowski, J. *J. Am. Chem. Soc.* **2009**, *131*, 6439–6444.
(35) Smith, D. P.; Bryant, A.; Quate, C. F.; Rabe, J. P.; Gerber, C.; Swalen, J. D. *Proc. Natl. Acad. Sci. U.S.A* **1987**, *84*, 969–972.
(36) Gregory, B. W.; Dluhy, R. A.; Bottomley, L. A. *J. Phys. Chem.* **1994**, *98*, 1010–1021.
(37) Carrer, D.; Kummer, E.; Chwastek, G.; Chiantia, S.; Schwille, P. *Soft Matter* **2009**, *5*, 3279–3286.
(38) Dietrich, C.; Bagatolli, L.; Volovyk, Z.; Thompson, N.; Levi, M.; Jacobson, K.; Gratton, E. *Biophys. J.* **2001**, *80*, 1417–1428.
(39) Rinia, H. A.; de Kruijff, B. *FEBS Lett.* **2001**, *504*, 194–199.
(40) Sullan, R. M. A.; Li, J. K.; Zou, S. *Langmuir* **2009**, *25*, 7471–7477.
(41) Brian, A. A.; McConnell, H. M. *Proc. Natl. Acad. Sci. U.S.A.* **1984**, *81*, 6159–6163.
(42) Johnson, J. M.; Ha, T.; Chu, S.; Boxer, S. G. *Biophys. J.* **2002**, *83*, 3371–3379.
(43) Richter, R. P.; Brisson, A. R. *Biophys. J.* **2005**, *88*, 3422–3433.
(44) Reviakine, I.; Brisson, A. *Langmuir* **2000**, *16*, 1806–1815.
(45) Cha, T.; Guo, A.; Zhu, X. *Biophys. J.* **2006**, *90*, 1270–1274.
(46) Leonenko, Z. V.; Carnini, A.; Cramb, D. T. *Biochim. Biophys. Acta, Biomembr.* **2000**, *1509*, 131–147.
(47) Lingler, S.; Rubinstein, I.; Knoll, W.; Offenhausser, A. *Langmuir* **1997**, *13*, 7085–7091.
(48) Rädler, U.; Mack, J.; Persike, N.; Jung, G.; Tampé, R. *Biophys. J.* **2000**, *79*, 3144–3152.
(49) Naumann, C. A.; Prucker, O.; Lehmann, T.; Ruhe, J.; Knoll, W.; Frank, C. W. *Biomacromolecules* **2002**, *3*, 27–35.
(50) Steltenkamp, S.; Muller, M. M.; Deserno, M.; Hennesthal, C.; Steinem, C.; Janshoff, A. *Biophys. J.* **2006**, *91*, 217–226.
(51) McKiernan, A. E.; Ratto, T. V.; Longo, M. L. *Biophys. J.* **2000**, *79*, 2605–2615.
(52) Ti Tien, H. *Adv. Mater.* **1990**, *2*, 316–318.
(53) Sinner, E.; Knoll, W. *Curr. Opin. Chem. Biol.* **2001**, *5*, 705–711.
(54) Naumann, R.; Schiller, S. M.; Giess, F.; Grohe, B.; Hartman, K. B.; Kärcher, I.; Köper, I.; Lübben, J.; Vasilev, K.; Knoll, W. *Langmuir* **2003**, *19*, 5435–5443.
(55) Garg, S.; Rühe, J.; Lüdtke, K.; Jordan, R.; Naumann, C. A. *Biophys. J.* **2007**, *92*, 1263–1270.
(56) Kiessling, V.; Crane, J. M.; Tamm, L. K. *Biophys. J.* **2006**, *91*, 3313–3326.
(57) Li, M.; Chen, M.; Sheepwash, E.; Brosseau, C. L.; Li, H.; Pettinger, B.; Gruler, H.; Lipkowski, J. *Langmuir* **2008**, *24*, 10313–10323.
(58) Chen, M.; Li, M.; Brosseau, C. L.; Lipkowski, J. *Langmuir* **2009**, *25*, 1028–1037.
(59) Zhang, L.; Booth, C. A.; Stroeve, P. *J. Colloid Interface Sci.* **2000**, *228*, 82–89.

Materials and Methods

Gold Surfaces. Gold-coated glass substrates ("11 × 11") were purchased from Arrandee. The backside of each substrate was cleaned using lab tissue and acetone to remove adhesive applied by the manufacturer for transport. Hydrogen flame emitted from a quartz pipet was used to heat the substrate until incandescence, producing gold grains several square micrometers in area with (111) surfaces exposed. The RMS roughness of each grain was ~0.15 nm as evaluated by atomic force microscopy (data not shown).

Hydrophilic Self-Assembled Monolayer. 11-Mercaptoundecanoic acid (MUDA) monolayers were chemisorbed on the flame-annealed gold surfaces at very high surface densities using a modified version of the experiment of Wang et al.[60] Briefly, the substrate was immersed in a 1 mM solution of MUDA (Sigma-Aldrich, 95%) and 5% (V/V) glacial acetic acid in ethanol immediately after flame-annealing and left overnight. Following incubation, substrates were rinsed with ~100 mL of solution containing 10% (V/V) amonium hydroxide and 90% (V/V) ethanol, then with ~300 mL ethanol, and then with copious amounts of 18 MΩ·cm H_2O (Barstead EASYpure II). The substrate was then dried under a stream of N_2 and epoxied to a clean 30 mm diameter round glass slide and left to cure in a laminar flow hood for 12 h. All ethanol was absolute, filtered through poly(tetrafluoroethylene) (PTFE) filters with pore size = 0.2 μm (Whatman) using a vacuum filtration flask (VWR). The MUDA modified Au substrates maintained their hydrophilicity longer than unmodified gold. Furthermore, after 12 h of exposure to air in the laminar flow hood (while the epoxy cured), the substrate would no longer hold a continuous sheet of water, but a thorough rinse with the ammonium hydroxide/ethanol solution, followed by a rinse with ethanol, and then with water restored the substrate's ability to hold a thin sheet of water at its surface.

Mica Substrates. Grade V1 muscovite mica discs (Ted Pella Inc., product no. 50) were epoxied to 30 mm diameter round glass discs and cured overnight in a lamellar flow hood. Immediately before lipid deposition, the sample was mounted in the fluid cell and hydrated with 50 °C 18 MΩ-·m H_2O. The mica was then cleaved under water using sharp tweezers, and the vesicle and salt solutions were applied immediately.

DOPC/Egg Sphingomyelin/Cholesterol Unilamellar Vesicles. 1,2-Dioleoyl-*sn*-glycero-3-phosphocholine, egg sphingomyelin, and ovine cholesterol (Avanti Polar Lipids) were mixed at 2:2:1 molar ratio at 1 mg/mL in chloroform (reagent grade, Sigma-Aldrich; filtered with 0.2 μm PTFE filters from VWR). Although fluorescence was not studied in this work, all aliquots contained fluorescent NBD-labeled phosphoethanolamine (1-palmitoyl-2-{12-[(7-nitro-2-1,3-benzoxadiazol-4-yl)amino]lauroyl}-*sn*-glycero-3-phosphoethanolamine) (Avanti Polar Lipids) at 0.2 mol %. Aliquots of 1 mL were dried under N_2 stream overnight, sealed, and stored at −20 °C until use. Dried lipid cake was rehydrated with phosphate buffered saline to 1 mg/mL at 60 °C and then vortexed to form multilamellar vesicles. The multilamellar vesicle suspension was refined to unilamellar vesicles by extrusion (mini extruder, Avanti Polar Lipids) at 60 °C using 0.1 μm PTFE filters following the manufacturer's directions. Each suspension was passed through the filter a minimum of 15 times, and always an odd number of times.

Vesicle Fusion. In an AFM fluid cell, the mounted substrate was incubated in a solution containing 100 μg of lipid in unilamellar vesicle form and $CaCl_2$ at a final concentration of 10 mM for 30 min. For the gold substrate, incubation occurred at room temperature, whereas for the mica substrate incubation occurred at ~50 °C. Afterward, the substrate was rinsed with ~200 mL of 18 MΩ·cm H_2O without allowing the substrate to dry or be exposed to air.

Atomic Force Microscopy (AFM) Imaging. Tapping mode AFM was performed in 18 MΩ·cm H_2O using an Asylum Research MFP3D (Asylum Research) instrument equipped with magnetic tip oscillation (iDrive). An oscillating AC current is passed from one base of a triangular, metalized cantilever to the other, creating an oscillating magnetic field, which causes the cantilever to oscillate in the static magnetic field supplied by a permanent magnet built into the cantilever holder. This produces amplitude and phase signals that are less noisy compared to traditional water-immersed AC-mode AFM, where cantilever oscillation is coupled strongly to resonances of the bulk fluid. It also necessitates the use of specialized gold-coated probes (nominal spring constant: 0.09 N/m). The round glass slide to which the sample was epoxied was mounted in a closed fluid cell (Asylum Research) according to the manufacturer's instructions.

Before immersion in the fluid cell, the tip was equilibrated in air for 10 min, and the cantilever spring constant calibrated by the thermal method after indentation into freshly cleaved mica. Following immersion of the tip into the fluid cell, the system was allowed to equilibrate in situ with the sample and water for 1 h prior to imaging.

Force Mapping and Automated Analysis. Force map data were collected using the instrument's included software. Indentations into the sample are made at even intervals across a fixed area, which allows information from each force curve to be mapped back to an (x,y) coordinate to produce images from the force data. Each indentation is triggered using a relative force value to ensure the same maximum indentation force is reached for each point. Force curves were analyzed offline using our own software written in IgorPRO 6.02 (Wavemetrics). A typical force indentation curve is shown in Figure 1 with an illustration of the interaction between the AFM tip and the bilayer. The contact point, and rupture events are found by determining the peaks in the second derivative of smoothed force versus Z curves (see Figure S1 in the Supporting Information). These data are used to automatically identify the presence of a breakthrough event and to record the rupture force. Each curve was also fit by the Sneddon model to obtain a Young's modulus value.

Elastic Indentation Model Fitting. Force veersus indentation data between the contact point and halfway to the breakthough point were fit by the Sneddon model, with the elastic modulus as the fitting parameter, and modified to account for differences between the physics of the model and the experiment. The Sneddon model assumes that the sample forms an infinite half-space below the tip, and thus differs from the experiment in which a thin soft material sits above a stiff substrate. Modifications to the model were made using two methods: the first according to Akhremitchev and Walker,[61] and the second according to Dimitriadis et al.[72] Neither correction method proved satisfactory, though indentation data collected on gold- and mica-supported bilayers can be compared when the same model is used to analyze each data set.

The Sneddon model relates the applied force (F) to the depth of indentation (δ) through experimental parameters such as probe tip geometry, and through material properties of the sample including Young's modulus (E) and Poisson's ratio (ν). For a parabaloid tip shape at low indentation depths, the model is mathematically identical to the Hertz model for a spherical indenter:

$$F = \frac{4}{3}\frac{E\sqrt{R}}{(1-\nu^2)}\delta^{3/2} \quad (1)$$

E was calculated as a fitting parameter assuming $\nu = 0.33$ and $R = 25$ nm.

Corrections to the model were made according to Akhremitchev and Walker,[61] where the correction factor to the fitted modulus can

(60) Wang, H.; Chen, S.; Li, L.; Jiang, S. *Langmuir* **2005**, *21*, 2633–2636.

(61) Akhremitchev, B. B.; Walker, G. C. *Langmuir* **1999**, *15*, 5630–5634.

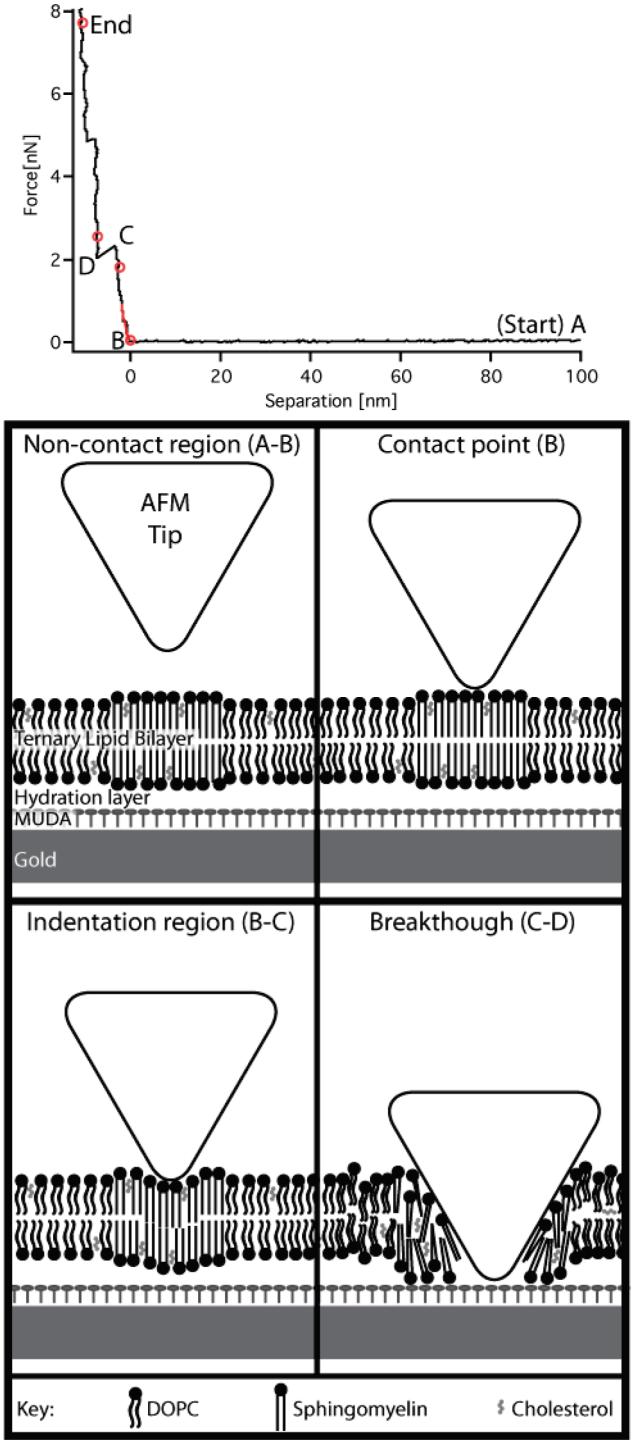

Figure 1. Typical AFM force indentation curve of the ternary lipid bilayer on gold (top) featuring a breakthrough event characteristic of these bilayers. Features of the indentation curve are labeled A through D. The four-panel diagram (not to scale) represents the interaction between the AFM tip and the lipid bilayer during the indentation process. Letters A−D refer to labeled features on the example indentation curve. The bilayer constituents (DOPC, egg sphingomyelin, and cholesterol) are drawn to represent the phase segregation of the DOPC from the egg sphingomyelin into l_d and l_o phases, respectively. The bilayer is supported by the mercaptoundecanoic acid (MUDA)-modified gold substrate through an assumed hydration layer.

be obtained graphically from a normalized force correction versus indentation curve. The correction factor depends on the ratio of Lamé coefficients between the thin material and the underlying substrate, as well as the normalized maximum indentation given by eqs 2 and 3, respectively:

$$\mu = \frac{E_1/[2(1-\nu_1)]}{E_2/[2(1-\nu_2)]} \tag{2}$$

$$\tilde{\delta}_{max} = \frac{\delta_{max} 2R}{h^2} \tag{3}$$

In eq 2, the subscripts 1 and 2 refer to the bilayer and the substrate, respectively. In eq 3, parabaloid tip geometry is assumed and δ_{max} is the maximum indentation of the fit, R is the radius of curvature, and h is the thickness of the bilayer, which we assume is 5 nm. The application of this correction is discussed in the following section.

Results and Discussion

Unlike many prior methods of producing lipid bilayers on gold surfaces, this method does not require headgroup modified phospholipids. Instead, widely studied DEC221 bilayers, which are known to phase segregate into raftlike domains,[1,37−40,62] are self-assembled on MUDA-modified flame-annealed gold. We cast the same bilayers onto mica for comparison on the basis of morphology and mechanical properties. We compare these results not only to each other but to the results of others who have cast these lipids on mica.[1,40] The primary intent, however, is not to quantify the true modulus of the bilayer as others have attempted, since doing so would require physically decoupling the bilayer from the solid support,[63] but rather to verify the coexistence of two lipid phases on gold and to characterize the bilayer in supported form. Briefly, we confirmed that a bilayer has formed on the gold substrate, and although there are differences in morphology of the domains, the modulus values of the domains are similar to those measured on mica.

Vesicle Fusion Requires Hydrophilic Surface. We explain the ability to form a DEC221 bilayer on the MUDA-modified gold, and the greater difficulty to do so on unmodified gold by differences in the hydrophilicity of the two substrates. The fusion of vesicles at a surface to form a supported bilayer can occur only on surfaces that are sufficiently hydrophilic. Otherwise, vesicles that settle on the surface tend to remain vesicular. On the other hand, when vesicles adsorb to strongly hydrophilic surfaces, they spread to maximize contact with the surface while causing increasing surface tension on the vesicle wall, and eventually rupture to form the supported bilayer. Adsorbed vesicles containing lipids with zwitterionic headgroups rupture readily on freshly cleaved mica, which is negatively charged, provided the buffer environment does not contain large molecular counterions that shield the surface charge.[45] The ability of adsorbed vesicles to spread on a surface can be estimated by the static contact angle made by a droplet of water on the surface. On freshly cleaved mica, the static contact angle of a drop of water is typically $< 5°$. The unmodified gold substrates can have static contact angles of $< 10°$ immediately after cleaning with oxygen plasma, UV-ozone, or piranha solution (Warning: Piranha reacts violently with organic material and should be handled with extreme care. Consult the materials saftety data sheet.), but these angles are short-lived due to rapid contamination. The MUDA-modified gold, either flame-annealed or not, showed static water contact angles of $< 10°$ (data not shown) and remains hydrophilic longer

(62) Popov, J.; Vobornik, D.; Coban, O.; Keating, E.; Miller, D.; Francis, J.; Petersen, N.; Johnston, L. *Langmuir* **2008**, *24*, 13502–13508.
(63) Ngwa, W. *Thin Solid Films* **2008**, *516*, 5045.

(perhaps by resisting fouling), and can be restored easily by rinsing with the ammonium hydroxide/ethanol solution, followed by rinsing with ethanol and then water. In fact, the same MUDA-modified substrate can be reused several times by thoroughly rinsing in this fashion. And like mica, a high-density self-assembled monolayer of MUDA has a net negative surface charge at neutral pH.

AFM Imaging and Lipid Phase Morphology on Gold. Because oriented mica substrates are atomically smooth, they are ideal supports for AFM studies of the phase behavior of lipid bilayers, which typically exhibit topographic contrast between phases of ~1 nm, depending on temperature and choice of lipids. Thermally deposited gold films on glass substrates, though useful for SPR and related techniques, are not suitable as substrates AFM studies of lipid bilayers because the root-mean-square (RMS) roughness of a polycrystalline gold film can be as high as 2.5 nm, which consequently dominates topographic images. The large (111) crystal faces of gold formed by flame-annealing can have RMS roughnesses < 1 nm when measured over single grains. Though better than as-deposited gold films, flame-annealed films can still contain topographic features that arise from the step-edges between (111) terraces on the crystal, which can range in height from 0.5 to 2 nm. Typical AFM height and phase images of MUDA-modified flame annealed gold are shown in Figure 2A and B, respectively. The lines that form trianglular shapes in the images are the crystal terraces of the (111) gold surface typical of flame-annealed gold surfaces.[64] Cross-sectional traces are provided in the Supporting Information. Although the topographic features of (111) Au complicate the interpretation of AFM height images relative to mica, such a treatment represents a great improvement over thermally deposited gold. Furthermore, the effect of topography in phase images and force maps is less pronounced, and consequently, we focus on these results. The topographic images and the effect of the substrate on phase segregation are also discussed.

An example of a DEC221 bilayer spontaneously formed on MUDA-modified, flame-annealed gold can be seen by AFM height and phase contrast in Figure 2C and D, respectively. Note that the region scanned in Figure 2C and D is not the same region shown in Figure 2A and B. The phase segregation of the bilayer into l_o and l_d domains is discernible both by height and phase contrast, though the step edges between (111) Au terraces make the distinction in the topography difficult to perceive.

What complicates the interpretation of the topography is that the boundaries of lipid phase domains tend to align with the edges of the terraces in a many cases. We hypothesize that the presence of topographic features on the scale of 1−2 nm (similar to the height mismatch expected between the l_o and l_d phases) can pin the migration of the phase boundaries. This consequently also affects the shape of the domains compared to how they appear on mica, which does not exhibit terracing. The coincidence of lipid phase boundaries with terrace edges can have either an additive or negating effect on the perceived height difference. Examples of these situations are discussed in the Supporting Information. Line traces of the height image show height differences between the l_o and l_d phases which range from 0.9 to 1.2 nm, which are comparable to accepted height differences on mica of about 0.8 nm, if the height differences between terraces are considered (see the Supporting Information). Thus, alternate mechanisms for contrast between the expected lipid phases is more reliable.

The morphology is more easily discernible in the phase image than in the height image. The l_o phase appears as the light gray features in the phase image, and the l_d phase appears as the dark gray regions. The coexistence of two lipid phases is verified by the breakthrough force map, which is discussed in the next section. Briefly, the presence of a breakthrough force event over most of the image area indicates good coverage by the bilayer. The map of the breakthrough force magnitudes reproduces the features in the phase image.

AFM Force Map of DEC221 on Gold. Force−indentation curves of the bilayers on gold were collected over a square grid in a selected area, and information such as the breakthrough force and Young's modulus can be mapped to an (x,y) coordinate. Force−indentation data were collected in a 64 × 48 grid over the same area as the AFM height image (Figure 2C), where Figure 2E and F shows maps of the Young's modulus and breakthrough force values extracted from the indentation data.

The breakthrough event is characteristic of an indentation curve collected over a bilayer. It occurs when a load is applied to the bilayer that is great enough to temporarily rupture the bilayer. At the point of rupture, the restoring force supplied by the bilayer is briefly lost, which is manifested in the force curve as a sudden drop in measured force (Figure 1). This discontinuity coincides with a peak in the second derivative of the force versus Z curve (see the Supporting Information), which is detected by our algorithm, and the breakthrough force is taken as the force value just before the rupture. Force curves over bare gold and MUDA-modified gold do not show the breakthrough event (data not shown). In Figure 2F, each point represents the magnitude of the force at the point where the tip ruptures the bilayer, or if no rupture event is detected, the maximum force is recorded but not displayed on the map since these points, which are typically defects in the bilayer, are not relevant to a breakthrough force analysis. Contrast between the l_o and l_d phases is clearly seen in Figure 2F, where features agree well with the AFM phase image (Figure 2D). Here, the force required to break through the l_o phase is higher than the force required to break through the l_d phase. This is expected because, in the sphingomyelin-rich l_o phase, the saturated acyl chains of the sphingomyelin allow closer packing of lipids than in the unsaturated DOPC-rich l_d phase,[65,66] therefore leading to stronger interactions between the chains and headgroups of neighboring molecules. Another manifestation of this packing effect is the higher T_m of saturated lipids compared to unsaturated lipids.[67,68]

Each point on the modulus map (Figure 2E) represents a single force−indentation curve where the Young's modulus is determined by a fit of the force versus separation curve between the contact point and halfway to the breakthrough point using the Sneddon model. If no breakthrough point was detected for a given curve, the model is fit to the first half of the entire indentation. Contrast between the two phases exists in the Young's modulus map as well, but it is less apparent than that in the breakthrough force map.

Contributions to the Young's modulus by each phase can be separated by considering their contributions to the breakthrough map. To do this, we first examine the histograms of the Young's modulus and breakthrough forces shown in Figure 2G and H, respectively. As was the case with the modulus map, the contributions to the modulus histogram made by the l_o and l_d phases cannot be clearly distinguished. On the other hand, their contributions to the breakthough force histogram are clear. Here we have excluded force curves that were not identified as

(64) Uosaki, K.; Shen, Y.; Kondo, T. *J. Phys. Chem.* **1995**, *99*, 14117–14122.
(65) Brown, D. A.; London, E. *J. Biol. Chem.* **2000**, *275*, 17221–17224.
(66) Litman, B. J.; Lewis, E. N.; Levin, I. W. *Biochemistry* **1991**, *30*, 313–319.
(67) Ladbrooke, B. D.; Chapman, D. *Chem. Phys. Lipids* **1969**, *3*, 304–356.
(68) Cronan, J. E.; Gelmann, E. P. *Bacteriol. Rev.* **1975**, *39*, 232–256.

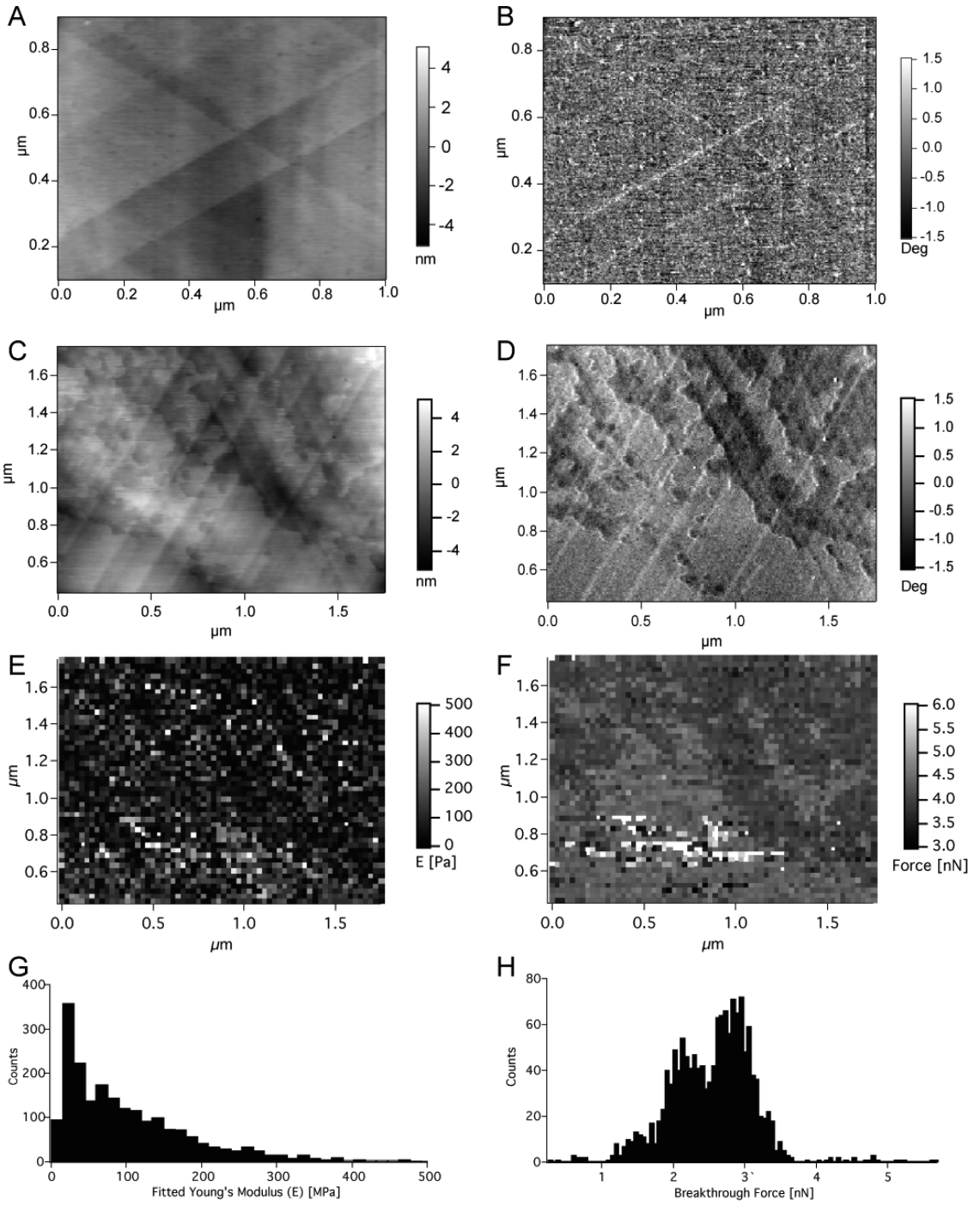

Figure 2. AC-mode AFM height (A) and phase (B) images of MUDA-modified, flame-annealed gold. Lines intersecting in triangular patterns are the terraces between (111) crystal planes of the Au. (C−H) AFM imaging and force mapping of DEC221 (DOPC/egg-SM/Chol mixed in 2:2:1 molar ratio) bilayers on MUDA-modified, flame-annealed Au at room temperature. AC-mode AFM height (C) and phase (D) images reveal phase segregation into liquid ordered (l_o) and disordered (l_d) phases. 64 × 48 force maps of the same area are processed to produce the Young's modulus and breakthrough force maps (E and F, respectively). Contrast between l_o and l_d phases is clearer in the breakthrough force map and follows the features on the phase image (D). (G and H) Histograms of the data mapped in (E) and (F), respectively. The histogram of breakthrough forces (H) has a largely bimodal distribution attributed to the l_o phase (peak at ~3 nN), and the l_d phase (peak at ~2.1 nN).

"breakthrough" events by the classification algorithm. The resulting bimodal distribution is then used as a guide to threshold the data. The cleft between the two peaks in the histogram is centered near 2.43 nN. We therefore separate all the breakthrough force curves into two categories: Those with breakthrough forces of ≥2.43 nN and <2.43 nN. Figure 3 shows the result of the separation. The features present in the separated Young's modulus maps (Figure 3C and D) show good agreement with the features attributed to their respective phases seen in Figure 2D. This indicates that the method of separation, however unsophisticated, is effective at isolating the two phases. The two separated Young's modulus histograms, therefore, mostly represent the two phases,

(69) Limpert, E.; Stahel, W. A.; Abbt, M. *BioScience* **2001**, *51*, 341.

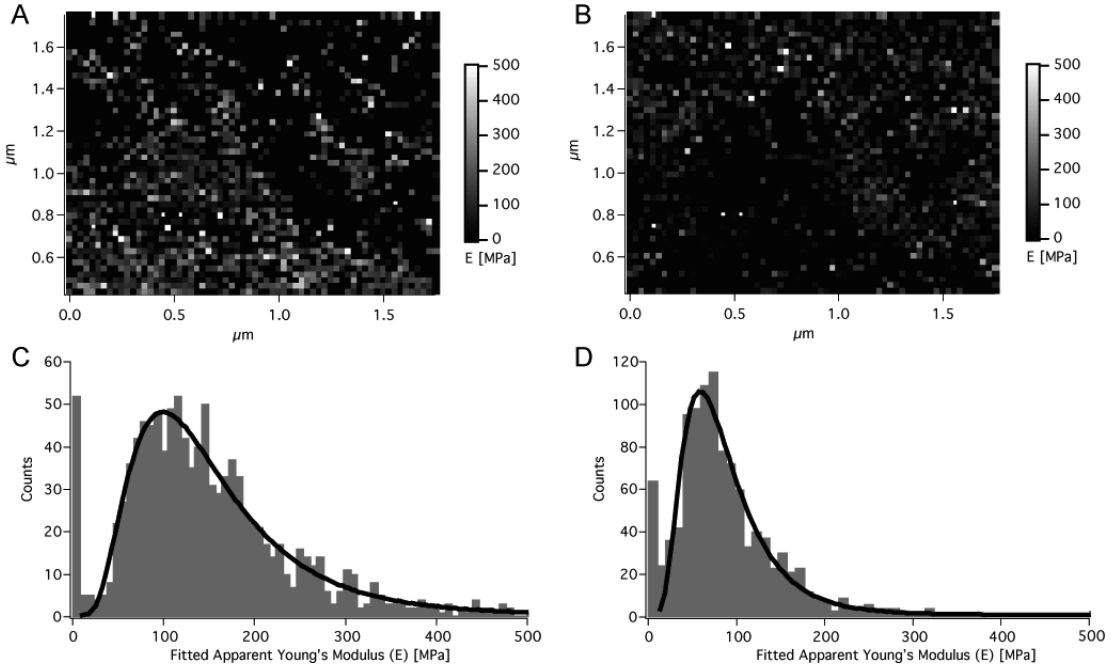

Figure 3. Breakthrough force contrast (see Figure 2D and F) used to separate data from the Young's modulus map (Figure 2C and E) into contributions from the l_o phase (A and C) and the l_d phase (B and D). Modulus maps (A) and (B) clearly correspond to features of the l_o phase and the l_d phase, respectively, indicating the data sorting is reasonable. (C and D) Histograms of data seen in modulus maps (A) and (B), respectively. Log-normal fits to the histograms (black lines in C and D) are used to determine the peak value: the average modulus of the l_o phase is 100 ± 2 MPa while that of the l_d phase is 59.8 ± 0.9 MPa.

respectively. Log-normal fits to each distribution[69−71] estimate the mean apparent Young's modulus of the l_o phase to be ~100 ± 2 MPa and that of the l_d phase to be ~59.8 ± 0.9 MPa.

These apparent moduli represent contributions to the modulus from the bilayer itself, in addition to contributions from the underlying gold substrate and perhaps even from the thin aqueous layer between them. This is a consequence of assumptions made in using the Sneddon model to fit the modulus. Specifically, the model assumes the tip is indenting into an infinite half-space of an elastic material, which is not representative of this supported lipid system. Indenting into a thin, soft film on a hard substrate can cause an overestimation of the modulus value because the stiffness of the substrate is felt through the soft film. Consequently, the apparent modulus value measured here is not the true modulus of the bilayer, and comparisons to other mechanical studies that attempt to physically decouple the bilayer from the substrate[63] are difficult to draw. As mentioned earlier, the intent here is to use the modulus values to help identify the lipid phases.

Comparison with Mica-Supported Bilayers. To help confirm the identity of the l_o and l_d phases on gold, we have repeated the experiment on mica substrates for comparison both by imaging and by force-mapping. Figure 4A shows a typical height-contrast contact-mode AFM image of DEC221 on mica, where the domains are clearly identified by height. Defects in the bilayer give rise to a third phase representing the bare mica substrate. In the breakthrough force map (Figure 4B), the bare mica patches appear as white because they are removed from this map by the classification subroutine (i.e., they were not identified as breakthrough events). Like the data collected on gold-supported samples, the contributions to the modulus map and histogram were separated by identifying a threshold value between the two peaks attributed to the two lipid phases in the breakthrough force histogram (Figure 4C). The two separated modulus maps (Figure 5A and B) show features that correspond well to the two lipid phases in the height image, indicating that the separation was reasonable. Fitting the separated modulus histograms to log-normal functions yielded mean apparent moduli of 164 ± 2 and 67 ± 1 MPa for the l_o and l_d phases, respectively.

Qualitatively, the lipids behave similarly on the two substrates. In both cases, phase segregation into the SM-enriched l_o and the DOPC-enriched l_d phases indicates that, like the mica surface, the gold substrate does not prevent spontaneous phase segregation. And as expected, denser packing of saturated SM molecules compared to unsaturated DOPC leads to higher apparent moduli and breakthrough forces on the l_o than the l_d phase on both substrates.

Overall, the apparent moduli for the lipid phases on both substrates are consistent with published results from a similar lipid system on mica.[40] The mechanical properties of the lipids, however, are known to depend strongly on lipid composition, temperature, thermal history, Ca^{2+} concentration, probe tip geometry, and the supporting substrate.[3,40,46] Although a quantitative comparison of mechanical properties was not the initial purpose of this work, such an analysis provides interesting insight into the relative contributions to the mechanical properties of the lipids from the van der Waals interactions between adjacent lipid chains, and from the electrostatic interactions between the headgroups and the substrate. The average apparent moduli for both phases are higher on mica than on gold. To account for this difference, consider the factors that play a role in the apparent modulus of the bilayer: the stiffness of the substrate, the thermal history of the lipids, and the surface charge density of the substrate.

(70) Cross, S. E.; Jin, Y.; Rao, J.; Gimzewski, J. K. *Nat. Nanotechnol.* **2007**, *2*, 780–783.
(71) Gerbal, F.; Laurent, V.; Ott, A.; Carlier, M.; Chaikin, P.; Prost, J. *Eur. Biophys. J.* **2000**, *29*, 134–140.
(72) Dimitriadis, E. K.; Horkay, F.; Maresca, J.; Kachar, B.; Chadwick, R. S. *Biophys. J.* **2002**, *82*, 2798–2810.

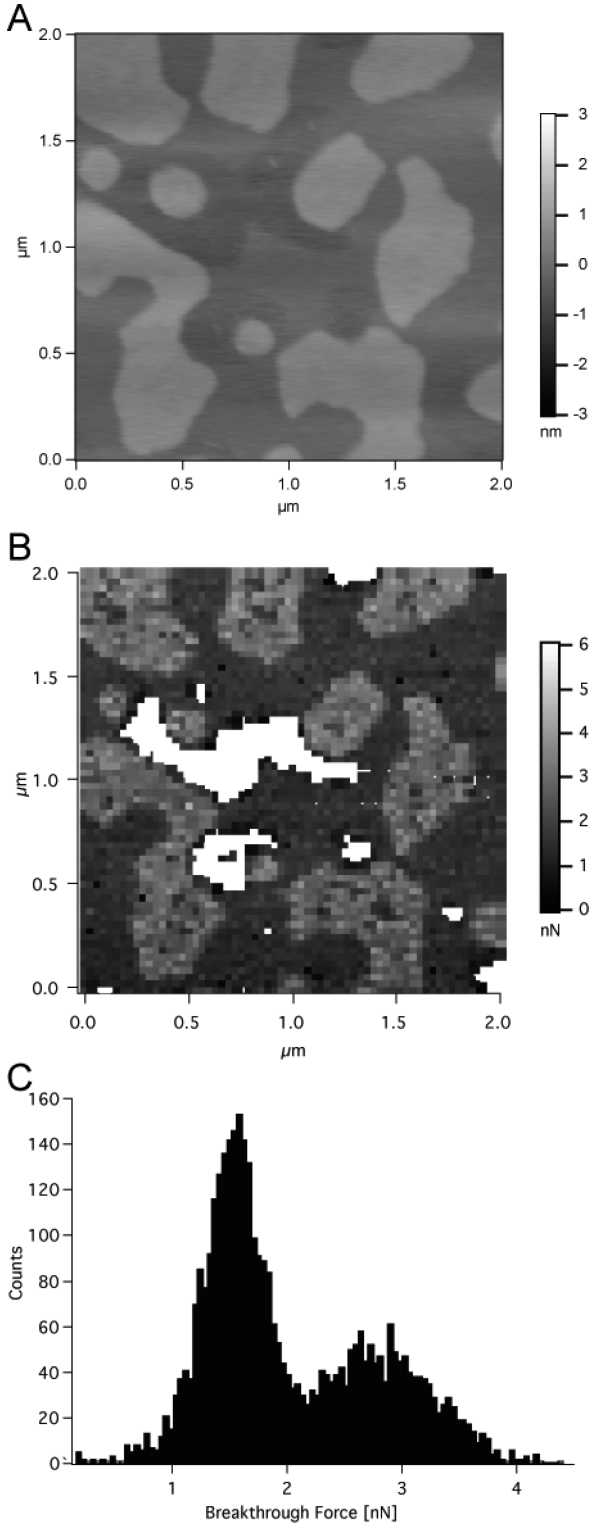

Figure 4. DEC221 on mica via vesicle fusion at 50 °C. Contact mode AFM height map (A) clearly shows two lipid phases l_o and l_d (higher and lower, respectively) as well as defects exposing bare mica. Breakthrough force map (B). White areas in (B) are excluded data points detected by software as nonbreakthrough events. Features in (B) correspond well with features in (A). Breakthrough force histogram shows characteristic bimodal distribution. Lower force peak corresponds to the l_d phase, while the higher force peak belongs to the l_o phase.

The Effect of the Substrate Stiffness on Apparent Modulus. That the apparent modulus is influenced by the supporting substrate can be expected intuitively. The presence of the support impedes out-of-plane bending of the bilayer in response to an applied load, and thus, the mechanical response can be understood in terms of the axial compression of the bilayer along with a lateral spreading of adjacent lipid molecules. Comparisons between the apparent moduli of lipid systems on different solid supports can be made if the relative contributions to the apparent modulus from the different substrates can be accounted for. The method of Akhremitchev and Walker[61] can be used to estimate the factor by which the modulus of a thin, soft layer over a hard substrate is overestimated by calculating the ratio of Lamé coefficients between the layer and the substrate, and transforming the force−indentation data to normalized coordinates as described therein. We approximate the ratio of Lamé coefficients (eq 2) as the ratio of moduli between the lipid layer and either the gold or mica substrate, considering that the other factors in the equation are small compared to this ratio. The average maximum indentation over which the modulus fits were calculated was ~1 nm, which from eq 3 produces a maximum normalized indentation of ~2. We estimate that these values represent an overestimation by a factor of >2.3. This factor is similar for bilayers on mica because the ratio of Lamé coefficients for mica-supported lipids is similar to that of gold-supported lipids, which is expected given the mismatch in moduli between the substrate and overlayer is quite similar. The modulus of mica is estimated between 50 and 180 GPa, which like gold is 3 orders of magnitude greater than the modulus of the bilayer measured here. Therefore, relative comparisons between apparent moduli on gold and mica are reasonable; that is, neither substrate will influence the deposited lipid much more than the other.

Other models exist to account for substrate interactions. For example, the model presented by Dimitriadis et al.[72] accounts for thin gel-phase samples that are either bonded or not bonded to a rigid support. Mathematically, the model modifies the Sneddon equation with a quartic equation in $\sqrt{\delta}$ where the coefficients differ depending on whether or not the film is bonded to the solid support. These coefficients depend nonlinearly on Poisson's ratio. This model, however, is not suitable for determining whether or not a layer is bonded to the substrate, but instead is more appropriate when the state of film/layer bonding can be determined.

Thermal History of Lipids. The phase behavior of lipid layers is complex, even for pure components. For example, X-ray scattering of multilayers of pure sphingomyelin analogues as well as natural sphingomyelin mixtures such as egg sphingomyelin (ESM) can exhibit coexisting phases under certain conditions.[73−75] Two gel-phases of ESM have been identified: interdigitated, and noninterdigitated, where the former consists of a subpopulation of molecules within the ESM mixture that have asymmetric lipid chains that can interdigitate at the midplane of the bilayer.[73] The addition of cholesterol at >30 mol % tends to inhibit temperature-dependent phase segregation, and is interpreted as preventing the formation of the interdigitated phase.[73] On the other hand, simultaneous X-ray diffraction and differential scanning calorimetry (DSC) of a synthetic, racemic sphingomyelin analogue suggests three phases are possible, depending on thermal history.[75] However, with its symmetric acyl chains, the SM analogue is not expected to form an interdigitated phase, which suggests alternate possibilities for the structure of the phases.

(73) Chachaty, C.; Rainteau, D.; Tessier, C.; Quinn, P. J.; Wolf, C. *Biophys. J.* **2005**, *88*, 4032–4044.
(74) Bruzik, K. S.; Tsai, M. D. *Biochemistry* **1987**, *26*, 5364–5368.
(75) Takahashi, H.; Okumura, Y.; Sunamoto, J. *Biochim. Biophys. Acta, Biomembr.* **2005**, *1713*, 40–50.

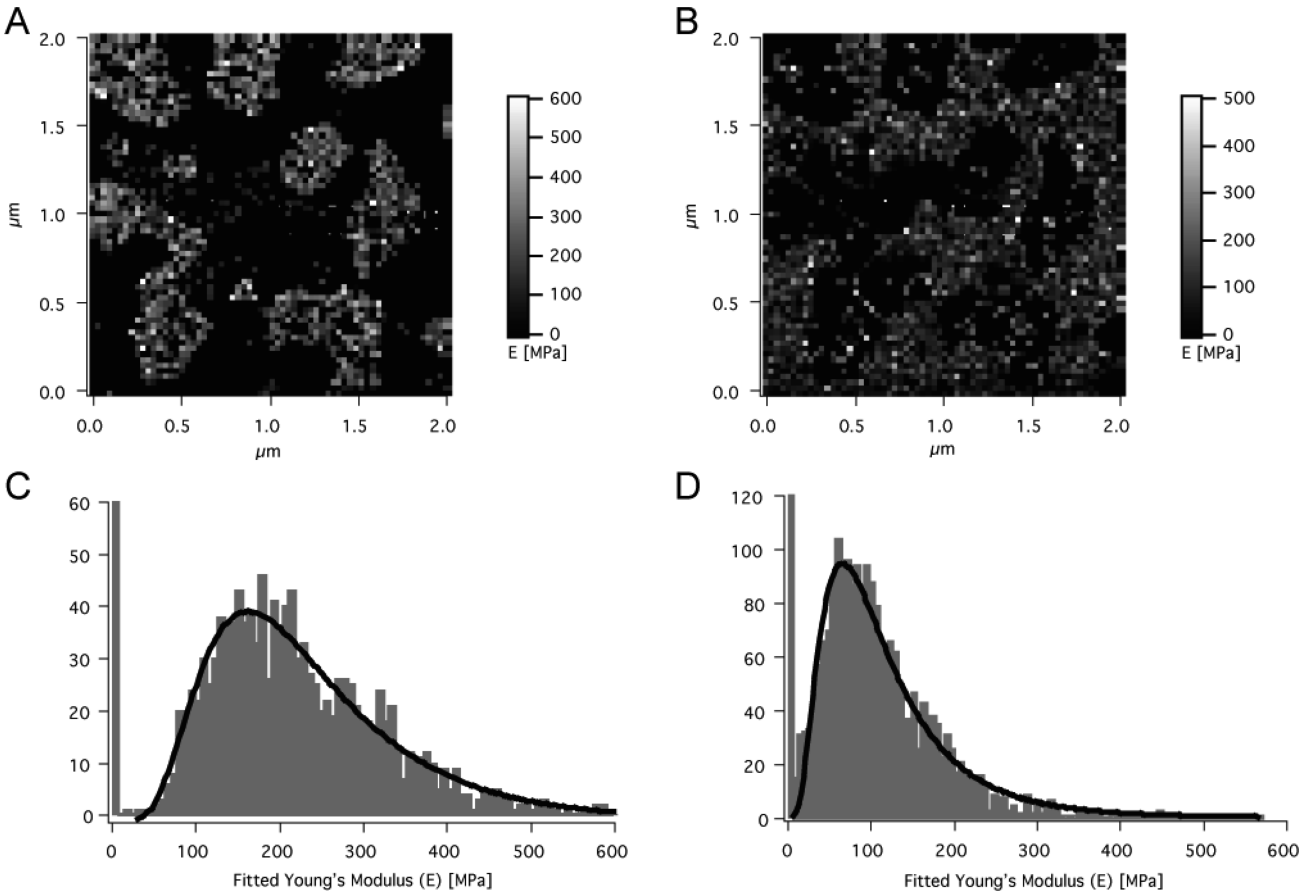

Figure 5. As with the lipid on gold, breakthrough force data (Figure 4C) used to sort modulus data into contributions from l_o and l_d phases. (A and C) Modulus map and associated histogram for the l_o phase. (B and D) Modulus map and histogram for the l_d phase. Average moduli acquired from log-normal fits to histogram are 164 ± 2 and 67 ± 1 MPa for the l_o and l_d phases, respectively. These results agree well with literature values.[40]

Furthermore, a stereochemically pure synthetic SM can also exhibit three distinct gel phases: one is stable and two are metastable, depending on thermal history, as revealed by DSC.[74] Since the lipids on the two substrates in the present study have undergone different thermal treatment, we do not expect to observe the same mechanical properties between the l_o phases of the two samples, since they may be in different phases. Although a more systematic study of the thermal-history-dependent behavior of these supported bilayers is warranted, some insight into the relative effect of thermal history and surface interaction can nevertheless be had as a consequence of this treatment.

The lipids on the mica were incubated at a temperature of 50 °C, which is higher than the melting temperature of all lipid components, whereas on the gold substrate the lipids were incubated at room temperature, which is above the melting temperature of the DOPC (−20 °C[76]) but below the melting temperature of ESM (41 °C[77]). Comparison of the apparent modulus values between the two phases on the two substrates reveals a greater difference between the moduli of the l_o phases than between the l_d phases. This result is not surprising, since in both cases the annealing temperature is above the melting temperature of the DOPC, which is believed to be the main component of the l_d phase, whereas only the mica sample was heated above the T_m of the ESM, which is enriched in the l_o phase. Thus, the thermal history is a greater factor in the properties of the l_o phase than in those of the l_d phase. Perhaps the higher temperature incubation has enabled the annealing of a metastable l_o phase into a stable phase. Other explanations for the difference between the moduli of the l_o phases cannot be excluded. For example, the difference in the shape of the l_o domains between the two samples suggests a difference in line tension at the phase boundaries,[78] which may affect the apparent modulus by affecting the packing of the tail groups or by changing the ability of the lipids to deform laterally.

Interestingly, the breakthrough force values of the l_o phase are ~3 nN for both samples, which suggests the breakthrough forces are not affected by the thermal history. The breakthrough forces recorded over the l_d phase, however, are higher on the gold-supported bilayer than on mica. Since the experiments occurred above the T_m of the DOPC for both samples, we do not expect the thermal history to be a factor in the properties of the l_d phase. This suggests that the breakthrough forces of the l_d phase are affected more by the properties of the substrate.

Surface Charge Density of Substrates. Electrostatic interactions between lipid headgroups and charged surfaces have been shown to have a profound effect on the formation of supported bilayers from vesicles. Furthermore, changes in effective surface charge affected by the presence of divalent ions can greatly impact bilayer formation and stability. Specifically, Ca^{2+} has been shown to promote the adsorption and rupture of lipid vesicles containing

(76) Schroeder, R.; London, E.; Brown, D. *Proc. Natl. Acad. Sci. U.S.A.* **1994**, *91*, 12130–12134.
(77) Samsonov, A. V.; Mihalyov, I.; Cohen, F. S. *Biophys. J.* **2001**, *81*, 1486–1500.
(78) García-Sáez, A. J.; Chiantia, S.; Schwille, P. *J. Biol. Chem.* **2007**, *282*, 33537–33544.

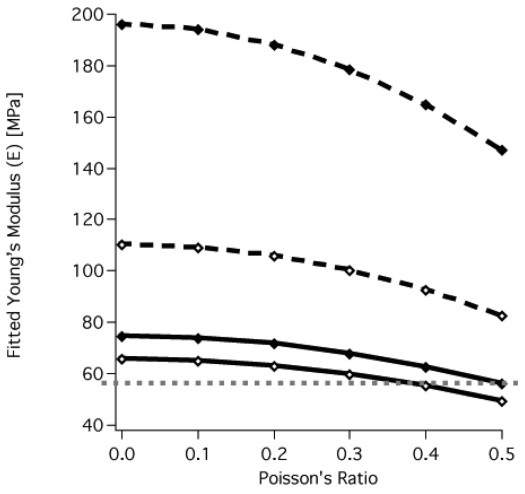

Figure 6. Effect of apparent Poisson's ratio on the fitted Young's modulus values. Solid and open markers are recalculated modulus values of the two phases on mica and gold, respectively. Black dashed and solid lines (guides to the eye) are the l_o and l_d phases, respectively. Consistent with the analysis discussed in the text, the lower apparent Poisson's ratio of the l_d phase on MUDA/gold than on mica could lead to the same modulus value of the actual bilayer, as indicated by the dotted gray line.

negative headgroups onto negatively charged surfaces by electrostatically bridging headgroup charges to charged sites on the surface. The same principle applies to zwitterionic headgroups, where the Ca^{2+} ion induces a dipole in the headgroup. In contrast, the efficiency of bilayer formation of cationic lipids on a net negative surface was not affected.[43]

The strong electrostatic coupling between the surface charges and the lipid headgroups suggests that the surface charge density must influence the stability of the bilayer. It follows that this interaction influences the ability of the bilayer to deform laterally under an applied load. Specifically, during AFM indentation, a load is applied perpendicular to the bilayer and substrate, and the bilayer is deformed both in the direction of the applied load as well as perpendicular to the applied load. The latter occurs by lateral reorganization of the lipid molecules. Strong coupling of the lipid molecules to the surface through electrostatic interactions can impede lateral relaxation and thus resist lateral deformation. The ability of a material to deform perpendicular to an applied load is captured in Poisson's ratio, ν, which can take on values between -1.0 and 0.5. Incompressible materials with $\nu = 0.5$ (such as rubber) expand perpendicular to an applied compressive load, while compressible materials with $\nu = 0$ (such as cork) do not strain in directions perpendicular to an applied load. Strong coupling between supported lipids and the underlying substrate would serve as a barrier to lateral deformation and thus reduce the apparent Poisson's ratio. Therefore, we expect the surface charge density to be a factor in determining the apparent modulus.

From estimates found in literature, the surface charge density of a COOH terminated monolayer on Au can have surface charge densities of up to 7.7×10^{-10} mol/cm^2 based on a perfect MUDA structure on (111) gold and complete ionization,[79] compared to a maximum of 3.3×10^{-10} mol/cm^2 based on the mica lattice structure.[80] It follows that the apparent Poisson's ratio of the lipid on the MUDA/gold surface should appear lower than that on the mica surface. Figure 6 illustrates the effect of the apparent Poisson's ratio on the fitted modulus. The modulus value is recalculated from the data for Poisson's ratios between 0 and 0.5. Poisson's ratios less than 0 were not considered because it is not apparent how the lipid bilayer could contract laterally under a compressive force. If we assume for the moment that the true modulus of the bilayer on both substrates is the same, then the difference in the apparent modulus may result from differences in the Poisson's ratio on the two substrates. For the l_d phase (two lower lines), the modulus could be the same on both mica and gold if the apparent Poisson's ratios were ~0.5 and ~0.38, respectively. Qualitatively, this is consistent with the conclusion that the MUDA/gold substrate, with its greater surface charge density, exhibits stronger coupling to the bilayer, leading to reduced lateral mobility and consequently lower apparent Poisson's ratios than on mica.

On the other hand, the differences between the moduli of the l_o phase on the two substrates (upper two lines) appear too great to be explained by differences in the apparent Poisson's ratio. This is not surprising because this implies that the intermolecular forces between the tightly packed sphingomyelin dominate over the surface effects. This is consistent with the expectation that thermal annealing affects the l_o phase much more than the l_d phase.

This view is also supported by the breakthrough force data. The breakthough event, where during indentation the tip reaches a critical force at which it penetrates the bilayer and makes contact with the underlying substrate, occurs via a breakage of intermolecular cohesive forces between adjacent lipids in the bilayer. The breakthrough force histograms on both mica and gold indicate that the breakthrough force over the l_o phase is similar on both substrates, around 3 nN, indicating a negligible effect of changing the substrate. Meanwhile, for the l_d phase, the peak breakthrough forces are ~1.5 and 2.1 nN on mica and gold, respectively. This supports the expectation that the more mobile l_d phase, with its weaker intermolecular forces, is more strongly influenced by electrostatic coupling of headgroups to the surface. Furthermore, the fact that the breakthrough force of the l_d phase is greater on gold than on mica is consistent with the greater surface charge density of the MUDA/gold substrate.

These considerations taken together suggest that the mechanical properties of the l_o phase are dominated by the thermal history and annealing due to the relatively large van der Waals forces present between the tightly packed alkyl chains. Meanwhile, the mechanical properties of the l_d phase, where the relative contribution from van der Waals forces is low, are dominated by the electrostatic coupling to the surface.

Conclusions

Previous methods of producing supported bilayers on gold have employed a variety of surface and lipid modifications in order to promote the adsorption and rupture of vesicles at the gold surface. Arguably, these modifications deviate from natural lipid bilayers. Although no supported lipid bilayer is identical to a cell membrane, ternary lipid mixtures of phosphatidylcholine lipids, sphingomyelin, and cholesterol are routinely used as model membranes supported by mica substrates because, like cellular membranes, they segregate into l_o and l_d phases. We have demonstrated the deposition of model, phase-segregated lipid bilayers (specifically a 2:2:1 mixture of DOPC, egg sphingomyelin, and cholesterol) on gold substrates using the standard vesicle fusion method without the use of charged or modified lipid headgroups. We also directly observe the phase segregation of the bilayers on gold using both AFM imaging and force indentation mapping. To facilitate AFM evaluation, the gold surfaces

(79) Smalley, J. F.; Chalfant, K.; Feldberg, S. W.; Nahir, T. M.; Bowden, E. F. *J. Phys. Chem. B* **1999**, *103*, 1676–1685.
(80) Qi, G.; Yang, Y.; Yan, H.; Guan, L.; Li, Y.; Qiu, X.; Wang, C. *J. Phys. Chem. C* **2009**, *113*, 204–207.

were smoothed by hydrogen flame annealing. Additionally, a high density mercaptoundecanoic acid self-assembled monolayer is grafted on the surface to improve the hydrophilicity and make the surface negatively charged to mimic mica.

The quality of the SLB on gold was evaluated in terms of the morphology and mechanical properties and compared to the same SLB on mica. Qualitatively, phase segregation was confirmed on both substrates from the AFM images. The l_o and l_d phases were indentified on gold by the height contrast as well as tapping mode phase contrast. Qualitatively, the mechanical properties, probed by force indentation mapping, were similar on both substrates: Statistically higher breakthrough forces were recorded over the l_o phase than the l_d phase on both substrates. Although the fitted moduli of the two phases differed between the gold- and mica-supported bilayers, they were of comparable magnitude. On both substrates, however, the l_o phase had a higher modulus than the l_d phase.

Further qualitative comparisons of the two samples revealed that the mechanical behavior of the l_o and l_d phases had different origins in terms of the relative contributions of van der Waals and electrostatic forces. The dominant electrostatic forces originate from coupling of the lipid headgroups to surface charges through divalent cations such as Ca^{2+}. van der Waals forces originate from intermolecular interactions between adjacent alkyl chains of the lipids. The properties of the l_o phase were dominated by strong van der Waals interactions attributed to tight packing of the lipids and, consequently, were affected more strongly by thermal history than by a change in surface charge density. Consequently, changing the surface charge density by changing the substrate did not affect the breakthrough force ($\sim$ 3 nN on both surfaces), which depends strongly on intermolecular interactions. The modulus of the l_o phase was higher on the surface where thermal annealing of the bilayer took place (164 vs 100 MPa). On the other hand, the mechanical properties of the l_d phase were less sensitive to thermal history and more sensitive to changes in surface charge density, indicating that the electrostatic coupling of the lipids to the surface dominate over the relatively weak van der Waals interactions. In this case, differences in both the modulus values and the breakthrough force values have their origin in the surface charge densities. The MUDA-modified gold substrate, with a higher surface charge density, supported an l_d phase with higher breakthrough forces ($\sim$2.1 vs $\sim$1.5 nN) and lower apparent Poisson's ratios (ν = 0.38 vs ν = 0.5). The lower apparent Poisson's ratio results from the decreased lateral mobility of lipids that inhibits lateral strain, resulting in lower calculated modulus values (62 vs 80 MPa). Though this is speculative, since it could be that the Young's modulus of these two disordered phases is simply different.

The methods employed herein can be extended in future experiments to better understand the role of surface charge density on the morphology and mechanical properties of SLBs, for example, by using mixed $-$COOH and $-$OH terminated monolayers to control surface charge density. Furthermore, the ability to form model membranes on metallic surfaces will improve the biological relevance of methods such as SPR in characterizing lipid bilayers. The demonstrated real-time sensitivity of SPR could have an impact on understanding the interaction dynamics between soluble analytes such as drugs and membranes and membrane-bound proteins.

Acknowledgment. We thank Dr. S. Zou, R. M. A. Sullan, and Dr. L. J. Johnston for helpful and constructive discussions. This work was supported by the Natural Sciences and Engineering Research Council of Canada.

Supporting Information Available: Plot showing the force versus Z piezo position and its second derivative; cross-sectional analysis of topography. This material is available free of charge via the Internet at http://pubs.acs.org.